JOURNAL OF CATALYSIS **161,** 115–122 (1996)
ARTICLE NO. 0168

Cu Containing Octahedral Molecular Sieves and Octahedral Layered Materials

Yan-Fei Shen,* Steven L. Suib,*,†,[1] and Chi-Lin O'Young‡,[1]

*Departments of *Chemistry and †Chemical Engineering and Institute of Material Science, U-60, University of Connecticut, Storrs, Connecticut 06269-3060; and ‡Texaco Research Center, Texaco, Inc., P.O. Box 509, Beacon, New York 12508*

Received March 10, 1995; revised December 18, 1995; accepted January 30, 1996

Manganese oxide octahedral molecular sieves (OMS) with Cu^{2+} in the tunnel (Cu-OMS-1) and octahedral layer (OL) manganese oxides with Cu^{2+} in the interlayer of buserite-like materials (Cu-OL-1) were prepared and characterized by X-ray diffraction, scanning electron microscopy/energy dispersive X-ray analysis, temperature programmed reduction, thiosulfate titrations, and volumetric adsorption of carbon monoxide (CO). The materials were tested as CO oxidation catalysts. Results show that autoclave treatment of Cu-OL-1 suspensions induces complete removal of chlorine as well as a change of the Cu/Mn ratio and average manganese oxidation state. Such changes depend on the initial MnO_4^-/Mn^{2+} ratio. At a ratio of 0.34–0.40, autoclave treatment increases the manganese oxidation state and the Cu/Mn ratio. At a ratio of 0.44, however, treatment decreases manganese oxidation state and the Cu/Mn ratio. A possible mechanism is proposed for the hydrothermal transformation of Cu-OL-1 to Cu-OMS-1. CO oxidation data show that Cu-OMS-1 has a CO conversion of 89–99% at 60–100°C, while Cu-OL-1 has almost no activity in the same temperature region. This dramatic difference is due to the fact that Cu-OMS-1 has more surface oxygen and a larger CO adsorption capacity, as compared to Cu-OL-1. Different structural properties may also contribute to the difference in catalytic activity, since the todorokite tunnel structure of OMS-1 is correlated with CO conversion. Blockage of the tunnels by water and tunnel collapse cause a significant decrease in CO oxidation. Kinetic studies of CO oxidation show that water vapor in the feed stream induces a small and reversible inhibition and that a positive reaction order is found with respect to CO partial pressure under these experimental conditions.

INTRODUCTION

Two types of manganese oxide octahedral molecular sieves (OMS-1 and OMS-2) have been successfully synthesized in our laboratory (1–6). OMS-1 is similar to the mineral todorokite, which has a tunnel size of about 6.9 Å. OMS-2 corresponds to a tunnel structure material called cryptomelane which has a tunnel size of 4.6 Å. These OMS materials may show unique catalytic properties like their natural corresponding minerals which are found in manganese nodules, which have been shown to be active catalysts for total oxidation of CO and hydrocarbons (7, 8) and for other reactions such as selective reduction of NO (9, 10), dehydrogenation (11), and demetallation (12, 13).

Octahedral layer (OL) materials have also attracted great attention recently, since these materials have unique physicochemical and catalytic properties, as compared to clays. Layered manganese oxides, consisting of MnO_6 single layer sheets and inorganic cations in the interlayer, show interesting properties, such as large cation exchange capacity for some inorganic cations (14), intercalation (15, 16), and transformation into tunnel structures (1–4, 17–19). Buserite, a layered manganese oxide with a (001) d-spacing of about 9.6 Å, has been prepared and transformed to a thermally stable todorokite (OMS-1) under mild hydrothermal conditions (1–4). The mechanism of such a transformation is not understood yet.

CO oxidation has been extensively investigated for several decades, because of its fundamental importance and for practical applications such as air purification, CO gas sensors, and in CO_2 lasers. Dispersed noble metals and mixed transition metal oxides are very active catalysts, such as platinized tin oxide (20), hopcalite (or amorphous $CuMn_2O_4$) (21–23), and highly dispersed Au on reducible transition metal (Ti, Fe, and Co) oxides (24–29). Hopcalite catalysts, however, suffer from severe deactivation problems (21).

The above-mentioned studies (1–29) and questions that have been generated from such work lead to the present study which focuses on applications of synthetic tunnel and layered manganese oxides. CO oxidation and the nature of the transformation mechanisms of buserite (OL-1) to todorokite (OMS-1) will be discussed. This is the first detailed report of the catalytic properties of OMS and OL materials.

EXPERIMENTAL

1. Sample Preparation

Manganese oxides with layered structures (OL-1) were prepared as follows: 50 ml of 5.0 *M* NaOH was added to

[1] To whom correspondence should be addressed.

0021-9517/96 $18.00

TABLE 1

Synthetic Cu-OL-1 and Cu-OMS-1

	0.34[a]	0.40[a]	0.44[a]
Name of Cu-buserite	Cu-OL-1 (34)	Cu-OL-1 (40)	Cu-OL-1 (44)
Name of Cu-todorokite	Cu-OMS-1 (34)	Cu-OMS-1 (40)	Cu-OMS-1 (44)

[a] Initial MnO_4^-/Mn^{2+} molar ratio.

40 ml of 0.50 *M* $MnCl_2$ aqueous solution at room temperature under vigorous stirring. A certain amount of 0.10 *M* $Mg(MnO_4)_2$ solution was then added dropwise to the stirred NaOH–$MnCl_2$ mixture. Three MnO_4^-/Mn^{2+} ratios, 0.34, 0.40, and 0.44, were chosen in order to clarify the controversial reported effects of manganese oxidation states on CO oxidation activity (22, 30, 31) and to understand the hydrothermal transformation of OL-1 to OMS-1. Table 1 lists the initial MnO_4^-/Mn^{2+} ratios and the designation of three Cu-OL-1 and three Cu-OMS-1 (*vide infra*) samples. After aging at room temperature for 4 days, the suspensions of the three samples were filtered and washed with distilled deionized water (DDW) until no chlorine ions were detected or until the pH of the filtrate was about 7. X-ray diffraction (XRD) patterns showed that the solid materials thus obtained were layered materials similar to Na-birnessite or Na-buserite.

The Na-birnessite suspensions were then exchanged with 300 ml of about 0.5 *M* aqueous solution of $CuCl_2$ at room temperature for about 2–3 h. The Cu^{2+}-exchanged products were then filtered and washed with DDW at least three times to obtain Cu-OL-1. Cu-OL-1 suspensions were autoclaved at 150–170°C for about 2 days to prepare Cu-OMS-1 materials. Cu-OMS-1 suspensions were filtered and washed with DDW three times and dried at room temperature in air.

2. X-Ray Diffraction

Cu-OMS-1 and Cu-OL-1 suspensions were spread on a glass slide and dried in air at room temperature. The dried films were calcined in air at different temperatures for 1 h. XRD patterns of fresh and calcined samples were obtained using a Scintag XDS-200 diffractometer with a Cu$K\alpha$ radiation source.

3. Scanning Electron Microscopy (SEM)/Energy Dispersive X-Ray (EDX) Studies

Sample powders were spread uniformly on carbon paste on an aluminum sample holder and subjected to SEM/EDX analyses using an Amray 1645 SEM and a Philips PV9800 EDAX spectrometer. The Super Quant program was used and at least five analyses were performed for quantitative measurements. Since elements lighter than Na cannot be accurately analyzed, data are reported as relative percentages.

4. Thiosulfate Titration

Average manganese oxidation states were determined by titration with sodium thiosulfate. A detailed procedure has been described elsewhere (32). A 10-mg sample dried at 120°C overnight was ground to fine powder and put in an Erlenmeyer flask. About 1 ml of NaOH/NaI solution (32 g NaOH, 60 g NaI, and 100 ml DDW) and 2 ml 1 : 5 sulfuric acid were added. The flask was shaken for about 10 min to dissolve the powder. The solution thus obtained was titrated with a 0.005 *N* sodium thiosulfate solution until the color of the solution was pale yellow. About 4 ml starch indicator solution (1 g in 500 ml boiling water) was added and more thiosulfate solution was added until the blue color disappeared. Three trials were done for each sample.

5. CO Volumetric Adsorption

The apparatus for volumetric adsorption of CO is schematically illustrated in Fig. 1. A 100-mg sample was loaded into the reactor (4) for thermal pretreatment at 300°C in vacuum for 3 h and then cooled down to room temperature for CO adsorption. CO gas was introduced into chamber 1 (V_1) and the CO pressure (P_1) was read by using a 122AA-01000AG pressure sensor (3). A Teflon valve connecting the sensor and the reactor was then opened to introduce CO for adsorption. After adsorption equilibrium was reached, the equilibrium pressure of CO (P_2) was recorded. The total CO adsorption amount was obtained according to the following equation where V_2 is equal to V_1 plus V_r:

$$n = (P_1V_1 - P_2V_2)/RT. \quad [1]$$

If there is no adsorption, $P_1V_1 = P_2V_2$. Physical adsorption can be measured by an adsorption–evacuation–readsorption cycle. Chemisorption is obtained by subtracting the amount obtained for physical adsorption from that obtained for total adsorption.

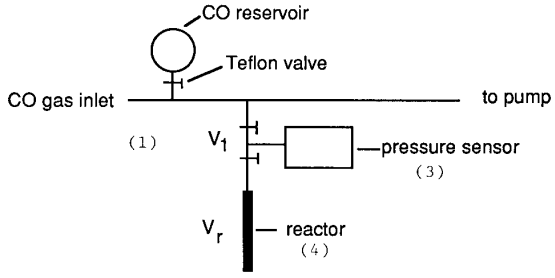

FIG. 1. Reactor for volumetric adsorption of CO.

6. CO Temperature-Programmed Reduction (TPR)

A 10-mg sample was loaded into a tubular quartz reactor. The sample was then heated up in a stream of CO/He (CO 5%) at a rate of 15°C/min. The CO_2, H_2O, and other high boiling point components were trapped with a liquid nitrogen/ethanol trap. Consumed CO was recorded using a Varian Aerograph Series 1400 gas chromatograph coupled with an HP 3396 Series II integrator.

7. Surface Oxygen Measurements

Surface oxygen species of Cu-OMS-1 and Cu-OL-1 were measured according to a method described in the literature (33). About 50 mg of the sample, 15 ml of phosphate buffer (7.0), and about 2 g of solid KI were placed in an Erlenmeyer flask. The mixture was vigorously stirred for about 6 h, filtered, and washed with methanol. The filtrate was acidified with 1.2 ml of 1.2 *N* HCl and the liberated iodine was titrated against 0.01 *N* sodium thiosulfate using starch as an indicator.

8. CO Oxidation

A 22-mg catalyst was loaded into a tubular glass microreactor and subject to a thermal pretreatment in flowing helium for 1 h. CO oxidation with air was then carried out at a space velocity of about 27,000 h^{-1}, a CO concentration of 10.7 vol.% in air, and at different temperatures. The effluent was analyzed with an HP 5880A series gas chromatograph with a Carboxen 1000 column.

RESULTS

1. Structural Transformation of Cu-OL-1 to Cu-OMS-1

Figure 2 shows the XRD patterns of three Cu-OL-1 samples with initial MnO_4^-/Mn^{2+} molar ratios of 0.34, 0.40, and 0.44, respectively. All the three samples show a strongest peak at 9.6 Å (near 9°2θ) and two peaks at 4.7–4.8 (near 19°2θ) and 2.4–2.5 Å (near 28°2θ). These peaks are due to buserite-type layered materials. A weak peak at about 7.1 Å (near 13°2θ) is also found, which is due to birnessite-type layered materials. Additional peaks at 5.8, 5.6, and 2.9 Å are detected. These three peaks appear to be related to copper hydroxychloride species, since these peaks are not detected in other cation (Mg^{2+}, Co^{2+}, Ni^{2+}, and Zn^{2+}) exchanged buserite or OL samples and they disappear when chlorine is removed during hydrothermal treatment (Fig. 3 and Table 2 below).

The three Cu-OMS-1 samples listed in Table 1 have the same XRD pattern. Therefore, only the XRD patterns of Cu-OMS-1 (40) calcined at different temperatures are shown in Fig. 3. Cu-OMS-1 (40) calcined at 100°C (Fig. 2a) has three peaks at about 9.6, 4.7, and 2.4 Å with relative intensities different from those of Cu-OL-1 (Fig. 1). The XRD patterns with the strongest peak at 4.7 Å have been

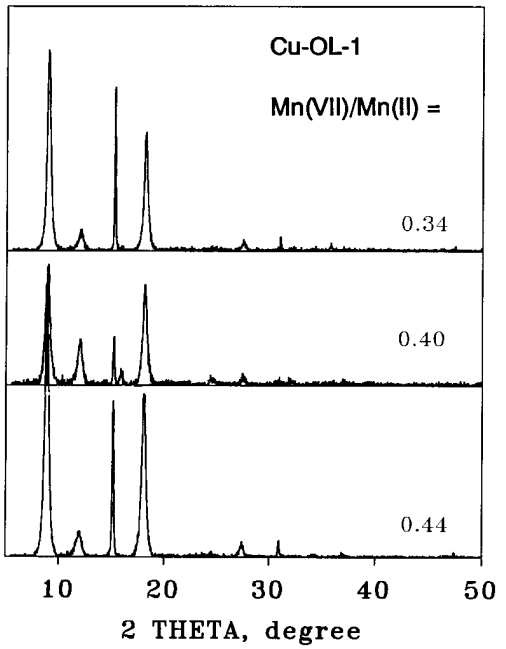

FIG. 2. XRD patterns of Cu-OL-1 samples with different MnO_4^-/Mn^{2+} ratios.

assigned to todorokite or OMS-1 (1–4). A small peak at 7.1 Å due to birnessite is occasionally observed, depending on preparation conditions. The three peaks at 5.8, 5.6, and 2.9 Å shown in Fig. 2 disappear after hydrothermal treatment (Fig. 3). Cu-OMS-1 (40) is intact after calcination in

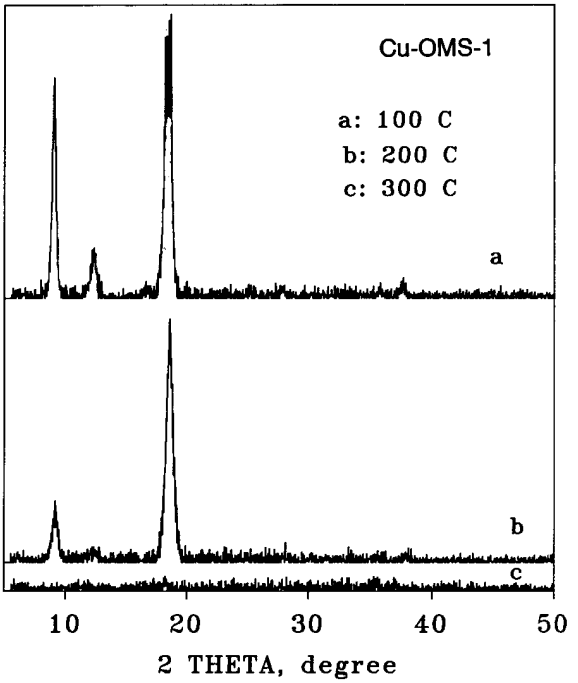

FIG. 3. XRD patterns of Cu-OMS-1 (40) calcined at different temperatures.

TABLE 2

SEM/EDX Data and Average Manganese Valency of Cu-OL-1 and Cu-OMS-1 Samples

Sample	Relative elemental percentage (at.%)			Cu/Mn molar ratio	Average manganese valency
	Cl	Mn	Cu		
Cu-OL-1 (34)	10.30	63.45	26.25	0.41	3.06
Cu-OL-1 (40)	8.82	61.99	29.19	0.47	3.22
Cu-OL-1 (44)	6.82	64.89	28.29	0.44	3.67
Cu-OMS-1 (34)	0	69.55	30.45	0.44	3.20
Cu-OMS-1 (40)	0	66.19	33.81	0.51	3.28
Cu-OMS-1 (44)	0	70.30	29.70	0.42	3.52

air at 200°C (Fig. 3b). Only a weak XRD peak is observed at $d = 4.8$ Å after calcination in air at 300°C (Fig. 3c), indicating that structural degradation starts to occur. Calcination at 400°C or higher temperature leads to the formation of spinel-type compounds, as described previously (3). Between 300 and 350°C surface area is retained and the peak at $d = 4.8$ Å is still observed, although at a very low intensity. The peak is difficult to observe in Fig. 3c due to the scaling with respect to data of Figs. 3a and 3b.

The above differences in XRD patterns between Cu-OL-1 and Cu-OMS-1 suggest the possibility that hydrothermal treatment induces changes in chemical composition and manganese oxidation states. SEM/EDX analyses and measurements of average manganese oxidation states were carried out to check this possibility. Data in Table 2 show that (1) a large amount of chlorine is detected in Cu-OL-1 and its content decreases with increasing MnO_4^-/Mn^{2+} ratio; (2) no chlorine is detected in Cu-OMS-1 samples; and (3) the Cu/Mn ratios and average manganese oxidation states increase or decrease concurrently after hydrothermal treatment, depending on the initial MnO_4^-/Mn^{2+} ratio. At a MnO_4^-/Mn^{2+} ratio of 0.34–0.40, Cu-OMS-1 (34) and Cu-OMS-1 (40) have a larger Cu/Mn ratio and manganese oxidation state than the corresponding OL-1 material, indicating that hydrothermal treatment increases the Cu/Mn ratio and manganese oxidation state. At a ratio of 0.44, Cu-OMS-1 (44) has a smaller Cu/Mn ratio and manganese oxidation state than Cu-OL-1 (44), indicating that hydrothermal treatment decreases the Cu/Mn ratio and the average manganese oxidation state with respect to the corresponding Cu-OL-1 material.

2. CO Oxidation

Table 3 shows the effect of MnO_4^-/Mn^{2+} molar ratios on the conversion of CO oxidation over Cu-OL-1. CO conversion is less than 1.5% at reaction temperatures of 150°C for all three samples. When reaction temperature is increased to 240°C, the conversion significantly increases to about

TABLE 3

Effects of MnO_4^-/Mn^{2+} Ratio on CO Oxidation over Cu-OL-1 Samples[a]

Catalyst	CO conversion (%)	
	240°C	150°C
Cu-OL-1 (34)	41.7	0
Cu-OL-1 (40)	63.0	1.0
Cu-OL-1 (44)	90.3	1.4

[a] A 22-mg catalyst was treated in He at 360°C for 1 h and then exposed to CO–air mixture at about 25,796 h^{-1} and 10.6% CO in air.

42–90%, depending on the MnO_4^-/Mn^{2+} ratio. CO conversion increases as the MnO_4^-/Mn^{2+} ratio increases at both reaction temperatures.

Table 4 shows the conversion of CO oxidation at 60–160°C over Cu-OMS-1, a commercial Pd/Al_2O_3 from United Catalysts, Inc., and a mixture of Cu-OMS-1 and γ-alumina at a 1 : 1 ratio by weight. Pd/Al_2O_3 and Cu-OMS-1 show 100% CO oxidation and Cu-OMS-1/alumina has about 98% conversion at 160°C. CO conversion is about 98–99% for Cu-OMS-1, 96% for Cu-OMS-1/Al_2O_3 mixture, and 3% for Pd/Al_2O_3, when reaction temperature is lowered to 100°C. At 80°C, Cu-OMS-1 and Cu-OMS-1/Al_2O_3 still have CO conversions of about 94 and 89%, respectively, while Pd/Al_2O_3 is completely inactive. At 60°C, the Cu-OMS-1 catalysts still have CO conversions of about 87–92%. These results indicate that Cu-OMS-1 catalysts are very active for CO oxidation at low temperature. The following sequence for CO conversion can be found from Tables 3 and 4: Cu-OMS-1 > Cu-OMS-1/Al_2O_3 ≫ Pd/Al_2O_3 ≫ Cu-OL-1. Unlike Cu-OL-1 catalysts, there is no obvious correlation between the MnO_4^-/Mn^{2+} ratio and CO conversion for Cu-OMS-1 catalysts.

Effects of pretreatment temperature on CO oxidation were investigated to study the relationships between the

TABLE 4

Effects of MnO_4^-/Mn^{2+} Ratio on CO Oxidation over Cu-OMS-1 and Pd/Al_2O_3 Catalysts[a]

Catalyst	CO conversion (%)			
	160°C	100°C	80°C	60°C
Cu-OMS-1 (34)	100	97.5	93.7	89.8
Cu-OMS-1 (40)	100	98.9	94.3	92.0
Cu-OMS-1 (44)	100	97.7	93.5	86.7
Cu-OMS-1 (40)/Al_2O_3 (50 wt%)	98	96.0	89.0	nd
Pd/Al_2O_3[b]	100	3	0	nd

Note. nd, not detected.

[a] A 22-mg catalyst was treated in He at 360°C for 1 h and then exposed to CO–air mixture at about 25,796 h^{-1} and 10.6% CO in air.

[b] Pd/Al_2O_3 (G-68) is from UCl.

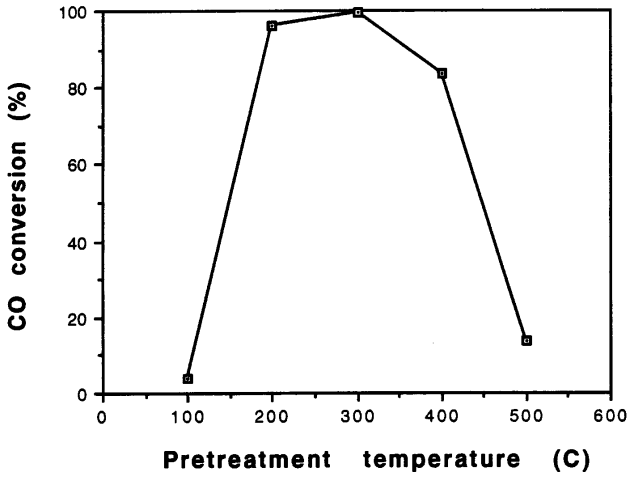

FIG. 4. Conversion of CO oxidation over Cu-OMS-1 (40) as a function of pretreatment temperature.

OMS-1 structure and the conversion in CO oxidation. Figure 4 shows results obtained at 80°C over Cu-OMS-1(40). CO conversion is about 5% for thermal pretreatment at 100°C and dramatically increases to about 98–100% for pretreatment at 200 and 300°C. The conversion decreases to about 82 and 15%, however, on further increasing the pretreatment temperature to 400 and 500°C, respectively.

Figure 5 shows the effects of CO concentration on CO conversion at 80°C over Cu-OMS-1 (40). At a concentration of 2% CO in air, about 93% conversion is obtained. The conversion increases to about 98% and almost 100% when CO concentration is increased to 3.2 and 10.7%, respectively. This indicates that the rate of CO oxidation under these experimental conditions is proportional to CO partial pressure.

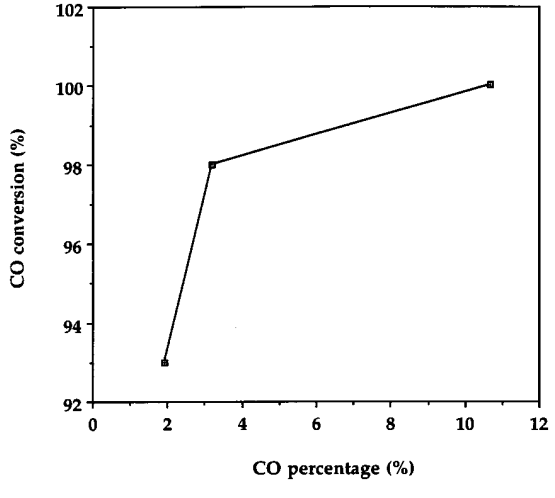

FIG. 5. Conversion of CO oxidation over Cu-OMS-1 (40) as a function of CO concentration.

TABLE 5

Effects of Water Vapor on the Conversion of CO Oxidation over Cu-OMS-1 (40)[a] Mixed with γ-Alumina (1 : 1)

Water vapor pressure (Torr)	CO conversion (%)
0	99.3
4.6	98.7
24	97.4

[a] A 22-mg Cu-OMS-1 (40)/γ-alumina was pretreated with He at 360°C for 1 h and subject to CO oxidation at 200°C.

Table 5 shows effects of water vapor on the conversion of CO oxidation at 200°C over Cu-OMS-1 (40)/γ-alumina. CO conversion slightly decreases from 99.3 to 98.7% when the CO/air stream contains water vapor at a pressure of 4.6 Torr over the catalyst. The conversion further slightly decreases to 97.4% when water vapor pressure is increased to about 24 Torr and does not change during the testing period of about 4 days. It increases to 99.3%, after the CO/air/water stream is switched back to the CO/air stream. These results indicate that (1) water vapor only has a slight inhibition effect on CO conversion, (2) water inhibition is reversible, and (3) Cu-OMS-1 catalysts have much longer lifetimes than hopcalite-type catalysts that are inactive after 36 h of reaction (21).

3. CO Adsorption/Desorption and Surface Oxygen

CO TPR experiments were carried out to elucidate why Cu-OMS-1 catalysts are much more active than Cu-OL-1. CO TPR spectra in Fig. 6 are considerably different for Cu-OL-1 (40) and Cu-OMS-1 (40). Cu-OMS-1 (40) shows a small CO TPD peak at about 130°C and two strong peaks at 230 and 300°C, while Cu-OL-1 (40) has five CO TPR peaks with similar intensities at about 160, 210, 280, 460, and 630°C. Though no peak assignments can be made, these significant differences may be related to surface oxygen

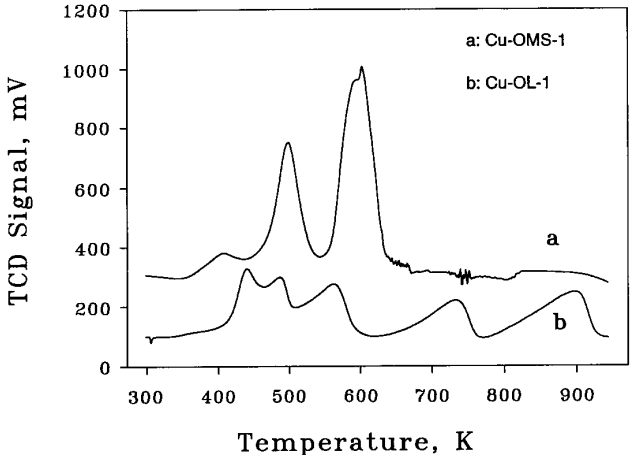

FIG. 6. CO TPR spectra of Cu-OL-1 (40) and Cu-OMS-1 (40).

TABLE 6

CO Adsorption on Cu-OMS-1 (40) and Cu-OL-1 (40) at Room Temperature

Sample	*P* (Torr)	CO adsorbed amount ($\times 10^{-5}$ mol/g)		Surface oxygen (meq/g)
		Chemisorption	Physical adsorption	
Cu-OMS-1 (40)	50.1	5.40	6.59	4.9
Cu-OL-1 (40)	50.1	0.14	3.59	3.2

species, which are believed to be the active species for complete oxidation of CO.

Volumetric adsorption data for CO in Table 6 show that physical adsorption of Cu-OMS-1 (40) is about 54% higher than that of Cu-OL-1 (40) and chemisorption of Cu-OMS-1 (40) is about 40 times as large as that of Cu-OL-1 (40). This indicates that Cu-OMS-1 has a larger surface area than Cu-OL-1 and also has much more active sites for CO chemisorption than Cu-OL-1.

Table 6 also shows data for surface oxygen species on Cu-OMS-1 (40) and Cu-OL-1 (40). Though the KI method described under Experimental is dependent on pH (33), data presented in Table 6 have been obtained under the same experimental conditions and thus are comparable. Table 6 clearly indicates that Cu-OMS-1 (40) has more surface oxygen species than Cu-OL-1.

DISCUSSION

1. Structural Transformation of OL-1 to OMS-1

Octahedral layered materials like buserite have been found to be thermally (34–36) and hydrothermally (1–4, 17–18, 37) transformed into tunnel structure manganese oxide materials having the todorokite or OMS-1 structure. Different sizes of tunnels can be produced, depending on the nature of cations in the interlayer of OL-1 and the transformation conditions. For example, K- and Ba-buserite materials are thermally transformed to hollandite-type materials (34–36), which have one-dimensional (2×2) tunnels consisting of two octahedral MnO_6 units edge shared by two other MnO_6 units. Smaller cations at high concentrations in buserite are transformed to bixbyite or hausmanite phases that are not tunnel structure materials. Under hydrothermal conditions, however, Ba-buserite is transformed to romanechite or psilomelane with a (2×3) tunnel structure (37), while smaller cations (Mg^{2+}, Co^{2+}, Cu^{2+}, and Zn^{2+}) give rise to todorokite or OMS-1 (1–4, 17, 18).

These transformation mechanisms of layered materials to tunnel structure materials have not been investigated, although a mechanism associated with "pillaring" between layer sheets has been suggested (34, 38). Our X-ray results of Figs. 2 and 3 and analytical data of Fig. 5 and Tables 2 and 6 suggest that the transformation is not just a simple pillaring process, but it involves liquid–solid and solid–solid chemical reactions as well as isomorphous substitution from compositional data of Tables 1 and 2 and other data. A model for the transformation is proposed, as schematically shown in Scheme I.

Our model basically involves the rearrangement of edge-sharing octahedral layer sheets, as supported by the facts that OL-1 does not dissolve during its transformation to OMS-1 and that OMS-1 partially preserves the plate-like morphology of OL-1 (2, 3, 17). The diagram of Scheme II basically describes the chemical reactions that may occur during the transformation. The initial step may be the cleavage of the Mn^{4+}-O(or Cl)-M (M=Mn^{2+}, Mn^{4+}, Cu^{2+}) bridge, which connects two octahedral units to form an edge-sharing buserite OL sheet. The existence of Cl^- in the bridge is supported by data in Table 2 and Fig. 2. Table 2 shows that the Cl^- content decreases with the MnO_4^-/Mn^{2+} ratio, indicating that the detected Cl^- is at least partially introduced by $MnCl_2$ and is most likely bound to framework cations. Figure 2 shows XRD peaks at 5.8, 5.6, and 2.9 Å. These peaks cannot be assigned to hydrated copper chlorides or other known copper and manganese compounds. A possible assignment is the above Cl^- bridge structure.

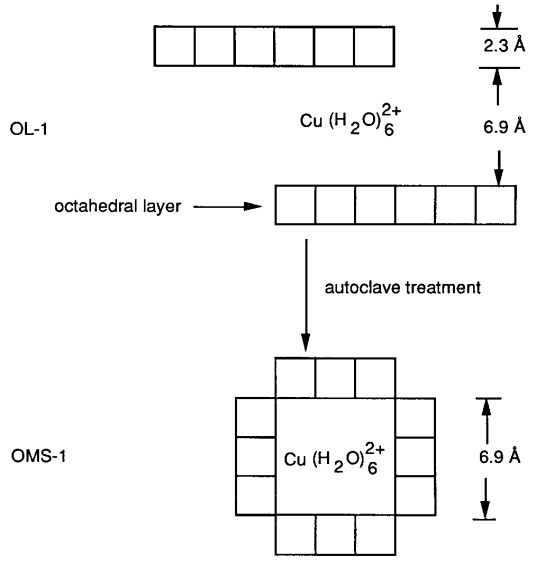

SCHEME I. Model for hydrothermal transformation of OL-1 to OMS-1.

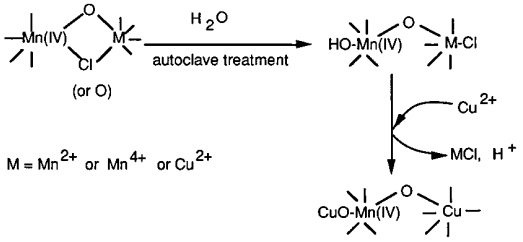

SCHEME II. Schematic diagram of possible reactions occuring during hydrothermal treatment.

When the bridge is broken, several other processes may take place. First, unsaturated Mn^{4+} may be hydrolyzed to form HO-Mn(IV)-O-M-Cl species. The OH^- group has been found to readily react with alkaline earth and divalent transition metal cations to form Cu^+-O-Mn(IV)-O-M-Cl species with concomitant release of H^+ (39–42). This may explain why alkaline earth and divalent transition metal cations in the tunnels of OMS-1 and other tunnel structure manganese oxides are not readily exchangeable. The released H^+, together with Cl^-, may dissolve extraframework MnO_2, leading to a lower manganese oxidation state (Table 2) and Cu/Mn ratio (Table 2) of Cu-OMS-1 (44) than those for Cu-OL-1 (44).

Cu^{2+} in the interlayer of Cu-OL-1 may also isomorphously substitute for Mn^{2+} during hydrothermal treatment, if there are enough Mn^{2+} cations in the framework of OL-1. Such isomorphous substitution leads to a higher Cu/Mn ratio and manganese oxidation state for crystalline (Fig. 3) Cu-OMS-1 (34) and Cu-OMS-1 (40) than for Cu-OL-1 (34) and Cu-OL-1 (40), as shown in Table 2.

Chlorine may be released during cleavage of the bridge species(I) which interacts with substituted Mn^{2+}, extraframework MnO_2, and Cu^{2+} to form soluble chlorides. This explains the absence of chlorine in the OMS-1 samples. Finally, the broken layer sheet may be rearranged under the direction of templating cations, leading to a tunnel structural material such as todorokite or OMS-1.

In summary, the hydrothermal transformation of OL-1 to OMS-1 is a complicated process, involving a possible cleavage of a Mn(IV)-O(or Cl)-M bridge structure such as species I, cation hydroxylation, and isomorphous substitution as well as partial dissolution of the solid phase.

2. CO Oxidation

All the Cu-OMS-1 catalysts are much more active (Table 4) for CO oxidation than Cu-OL-1 (Table 3). This is attributed to several factors. The first factor is CO adsorption, as shown in Table 6. More physical adsorption of CO on Cu-OMS-1 is observed perhaps due to the larger surface area of Cu-OMS-1 as compared to Cu-OL-1. Cu-OMS-1 has CO chemisorption about 40 times greater than Cu-OL-1, indicating that surface structure and composition of these catalysts are more important than surface area for CO oxidation. Therefore, surface oxygen is considered to be a secondary factor for explaining differences in activity. TPR data of Fig. 6 clearly show differences in amounts and types of surface oxygen species of Cu-OL-1 and Cu-OMS-2.

Results of Table 6 show that Cu-OMS-1 has more surface oxygen species than Cu-OL-1, suggesting a critical role of surface oxygen species in CO oxidation. Other reports also support an important role of surface oxygen and OH^- species as well as the so-called active bulk oxygen in CO oxidation (22, 43, 44). A third reason for enhanced CO oxidation may arise from synergistic effects of manganese and copper. The formation of Cu-O-Mn bonds and incorporation of Cu^{2+} into the framework during hydrothermal transformation may reinforce such effects. Such synergistic effects find support from the fact that homogeneous mixing of copper and manganese in hopcalite materials produces much better CO oxidation activity than poor mixing (21). In summary, the high CO oxidation activity of Cu-OMS-1 is due to its large CO adsorption capacity, a large amount of surface oxygen species, and synergistic effects of manganese and copper.

CO oxidation activity also appears to be related to the tunnel structure of OMS-1. CO oxidation activity (Fig. 4) and the amounts of cyclohexane adsorption (3) are maximized when Cu-OMS-1 is thermally pretreated at 200–300°C (*vide infra*). This indicates that CO oxidation is related to the OMS-1 tunnel structure. CO oxidation activity is small, when pretreatment temperature is not high enough to remove tunnel water. High temperature (≥350°C) pretreatment destroys the tunnel structure (3) and decreases the activity for CO oxidation (Fig. 4). There is still some crystallinity for the material heated to 300°C and porosity is retained on the basis of BET data. Note that all catalytic data of Tables 3 and 4 are at temperatures considerably lower than those (>300°C) that lead to loss of structure and porosity.

CO oxidation kinetics have been extensively investigated. Figure 5 and Table 5 give preliminary results about effects of CO concentration and water vapor on CO conversion. The reaction order is found to be dependent on CO partial pressure in the CO concentration region of 2–10.7%. A measurable reversible inhibition effect of water vapor appears to indicate that the effect is due to reaction kinetics rather than strong competition for adsorption sites on the catalyst.

The average relative rates of oxidation of CO at 80°C are 0.115 mol/g catalyst h^{-1} for Cu-OMS-1, 0.109 mol/g catalyst h^{-1} for Cu-OMS-1/Al_2O_3, 0 for Pd/Al_2O_3, and 0 for Cu-OL-1. At 60°C, only Cu-OMS-1 is active and the rate drops to 0.112 mol/g catalyst h^{-1}. Note that these rates are average rates and can have a large variation due to the high conversions and high space velocities which may change considerably with small variations in partial pressure. Nev-

ertheless, these turnover frequencies give some idea of the relative rates of activity for these different OMS and OL materials.

CONCLUSIONS

Cu-OL-1 with different MnO_4^-/Mn^{2+} ratios has been successfully transformed into Cu-OMS-1 under mild hydrothermal conditions. The transformation may involve solid–liquid and solid–solid reactions, such as cleavage of a Mn(IV)-O(or Cl)-M bridges, cation hydroxylation, and isomorphous substitution as well as partial dissolution of the solid phases.

Cu-OMS-1 and Cu-OL-1 show significant differences in physicochemical and catalytic properties. Compared to Cu-OL-1, Cu-OMS-1 has a much higher CO oxidation activity, a much larger CO adsorption capacity, a larger amount of surface oxygen species, and different CO reduction behavior.

CO oxidation over Cu-OMS-1 is proportional to CO concentration in the CO concentration region of 2–10.7%. Water vapor slightly inhibits CO oxidation and this inhibition process is reversible. Above 300°C, the structure of Cu-OMS-1 collapses and leads to a decrease in the rate of CO oxidation.

ACKNOWLEDGMENTS

We thank the Department of Energy, the Office of Basic Energy Sciences, Division of Chemical Sciences and Texaco, Inc., for support of this research.We thank Dr. Wen-Qing Xu for collecting CO TPR data.

REFERENCES

1. Shen, Y.-F., Zerger, R. P., Suib, S. L., McCurdy, L., Potter, D. I., and O'Young, C.-L., *J. Chem. Soc. Chem. Commun.* 1213 (1992).
2. Shen, Y.-F., Zerger, R. P., Suib, S. L., McCurdy, L., Potter, D. I., and O'Young, C.-L., *Science* **260**, 511 (1993).
3. Shen, Y.-F., Suib, S. L., and O'Young, C.-L., *J. Am. Chem. Soc.* **116**, 11020 (1994).
4. Shen, Y.-F., Suib, S. L., and O'Young, C.-L., In preparation.
5. O'Young, C.-L. *in* "Expanded Clays and Other Microporous Solids" (Occelli and H. Robson, Eds.), p. 333. Van Nostrand Reinhold, New York, 1992.
6. DeGuzman, R., Shen, Y.-F., Suib, S. L., Shaw, B. R., and O'Young, C.-L., *Chem. Mater.* **5**, 1395 (1993).
7. Weisz, P. B., U.S. patent 3,214,236 (1965); *J. Catal.* **10**, 407 (1968).
8. Matsuo, K., Nitta, M., and Aomura, K., *J. Jpn. Pet. Inst.* **22**, 212 (1979).
9. Wu, S. C., and Chu, C., *Atm. Environ.* **6**, 309 (1972).
10. Matsuo, K., Nitta, M., and Aomura, K., *J. Jpn. Pet. Inst.* **22**, 384 (1979).
11. Fischer, R. H., Jarwood, W. E., and Heineman, H., *Ind. Eng. Chem. Proc. Des. Dev.* **15**, 570 (1976).
12. Nitta, M., Matsuo, K., and Aomura, K., *Chem. Lett.* 125 (1979).
13. Chang, C. D., and Silvestri, A. J., *Ind. Eng. Chem. Proc. Des. Dev.* **13**, 315 (1974).
14. Wadsley, A. D., *J. Am. Chem. Soc.* **72**, 1781 (1950).
15. Wong, S.-T., and Cheng, S., *Inorg. Chem.* **31**, 1165 (1992).
16. Paterson, E., *Am. Mineral.* **66**, (3–4), 424 (1981).
17. Golden, G. C., Chen, C. C., and Dixon, J. B., *Science* **231**, 717 (1986).
18. Golden, G. C., Chen, C. C., and Dixon, J. B., *Clays Clay Miner.* **35**(4), 271 (1987).
19. Hirano, S. I., Narita, R., and Naka, S., *J. Crystal Growth* **55**, 595 (1981).
20. Gardner, S. D., Hoflund, G. B., Schryer, D. R., and Upchurch, B. T., *J. Phys. Chem.* **95**(2), 835 (1991).
21. Puckhaber, L. S., Cheung, H., Cocke, D. L., and Clearfield, A., *Solid State Ionics* **32/33**, 206 (1989).
22. Kanungo, S. B., *J. Catal.* **58**, 419 (1979).
23. Lamb, A. B., Bray, W. C., and Frazer, J. C. W., *J. Ind. Eng. Chem.* **12**, 213 (1920).
24. Haruta, M., Tsubota, S., Kobayashi, T., Kageyama, H., Genet, M. J., Delmon, B., *J. Catal.* **144**, 175 (1993).
25. Gardner, S. D., Hoflund, G. B., Upchurch, B. T., Schryer, D. R., Kielin, E. J., and Schryer, J., *J. Catal* **129**, 114 (1991).
26. Tanielyan, S. K., and Augustine, R. L., *Appl. Catal. A* **85**, 73 (1992).
27. Knell, A., Barnickel, P., Barker, A., and Wokaun, A., *J. Catal.* **137**, 306 (1992).
28. Lin, S. D., Bollinger, M., and Vannice, M. A., *Catal. Lett.* **17**, 245 (1993).
29. Sze, C., Gulari, E., and Demczyk, B. C. *in* "Nanophase and Nanocomposite Materials," MRS Symposium Proceedings, Vol. 286, p. 143, 1993.
30. Veprek, S., Cocke, D. L., Kehl, S., and Oswald, H. R., *J. Catal.* **100**, 250 (1986).
31. Schwab, G. M., and Kanungo, S. B., *Z. Phys. Chem. N. F.* **107**, 109 (1977).
32. Murray, J. W., Balistieri, L. S., and Paul, B., *Geochim, Cosmochim, Acta.* **48**, 1237 (1984).
33. Uchijima, T., Takahashi, M., and Yoneda, Y., *J. Catal.* **9**, 403 (1967).
34. Chen, C.-C., Golden, D. C., and Dixon, J. B., *Clays Clay Miner* **34**, 565 (1986).
35. Golden, D. C., Chen, C.-C., and Dixon, J. B., *Clays Clay Miner* **34**, 511 (1986).
36. Giovanoli, R., and Balmer, B., *Chimia* **35**, 53 (1981).
37. Wadsley, A. D., *Am. Mineral.* **35**, 485 (1950).
38. Arrhenius, G. O., and Tsai, A. G., *SIO Ref. Series* **81**(28), 1 (1981).
39. Murray, D. J., Healy, T. W., and Fuerstenau, D. W., *Adv. Chem. Ser.* **79**, 74 (1968).
40. Murray, J. W., *Geochim. Cosmochim. Acta.* **39**, 505 (1975).
41. Loganathan, P., and Burau, R. G., *Geochim. Cosmochim. Acta.* **37**, 1277 (1973).
42. Gadde, R. R., and Laitinen, H. A., *Anal. Chem.* **46**, 2022 (1974).
43. Kobayashi, M., Matsumoto, H., and Kobayashi, H., *J. Catal.* **21**, 55 (1971); **27**, 100 (1971).
44. Hasegawa, S., Yasuda, K., Mase, T., and Kawaguchi, T., *J. Catal.* **46**, 125 (1977).